Electronic Supplementary Information (ESI) for

Transformative route to nanoporous manganese oxides of controlled oxidation states with identical textural properties

Jae Hwa Lee,[a,‡] Young Jin Sa,[a,‡] Tae Kyung Kim,[a] Hoi Ri Moon*[a] and Sang Hoon Joo*[b]

[a] Department of Chemistry, Ulsan National Institute of Science and Technology (UNIST), 50 UNIST-gil, Ulsan 689-798, Republic of Korea. E-mail: hoirimoon@unist.ac.kr

[b] School of Energy and Chemical Engineering and KIER-UNIST Advanced Center for Energy, Ulsan National Institute of Science and Technology (UNIST), 50 UNIST-gil, Ulsan 689-798, Republic of Korea. Fax: 82-52-217-2509; Tel: 82 52 217 2522; E-mail: shjoo@unist.ac.kr

Table S1. X-ray crystallographic data of Mn-MOF.

Compound	Mn-MOF
formula	$Mn_2C_{16}N_2O_{10}H_{24}$
crystal system	*Triclinic*
space group	*P-1*
fw	514.25
a, Å	6.473(13)
b, Å	7.970(16)
c, Å	10.577(2)
α, deg	101.69(3)
β, deg	102.84(3)
γ, deg	105.70(3)
V, Å^3	491.7(17)
Z	1
ρ_{calcd}, g cm^{-3}	1.737
temp , K	100(2)
λ, Å	0.69999
μ, mm^{-1}	1.343
goodness-of-fit (F^2)	1.093
F(000)	264
reflections collected	5533
independent reflections	2865 [*R*(int) = 0.0122]
completeness to θ_{max}, %	88.0
data/parameters/restraints	2865/136/0
θ range for data collection, deg	3.42-33.96
diffraction limits (*h*, *k*, *l*)	$-9 \le h \le 9$, $-11 \le k \le 11$, $-15 \le l \le 15$
refinement method	Full-matrix least-squares on F^2
R_1, wR_2 [$I>2\sigma(I)$]	0.0379[a], 0.1079[b]
R_1, wR_2 (all data)	0.0384[a], 0.1082[b]
largest peak, hole, eÅ^{-3}	0.973, -0.925

[a] $R = \Sigma||Fo| - |Fc||/\Sigma|Fo|$. [b] $wR(F^2) = [\Sigma w(Fo^2 - Fc^2)^2/\Sigma w(Fo^2)^2]^{1/2}$ where $w = 1/[\sigma^2(Fo^2) + (0.0573P)^2 + (0.0000)P]$, $P = (Fo^2 + 2Fc^2)/3$.

Table S2. Selected bond distances (Å) and angles (deg) of Mn-MOF.

Mn(1)-O(1)	2.1177(15)	Mn(1)-O(2)	2.1204(16)
Mn(1)-O(3)	2.1097(14)	Mn(1)-O(4)	2.1246(14)
Mn(1)-O(5)	2.0771(18)	Mn(1)-Mn(1)$^{\#1}$	3.0511(11)
O(1)-Mn(1)-O(2)	157.55(7)	O(1)-Mn(1)-O(3)	85.21(6)
O(1)-Mn(1)-O(4)	88.96(6)	O(1)-Mn(1)-O(5)	99.23(7)
O(2)-Mn(1)-O(3)	89.29(6)	O(2)-Mn(1)-O(4)	87.98(6)
O(2)-Mn(1)-O(5)	103.09(7)	O(3)-Mn(1)-O(4)	157.81(6)
O(3)-Mn(1)-O(5)	98.18(7)	O(4)-Mn(1)-O(5)	103.89(7)

Symmetry transformation used to generate equivalent atoms:
$^{\#1}$, -x+2,-y+1,-z+1

Table S3. BET surface areas and total pore volumes obtained from nitrogen adsorption analysis, and the nanocrystalline sizes of nanoparticles composing frameworks of manganese oxides.

Sample	BET surface area[a] ($m^2\ g^{-1}$)	Pore volume[b] ($cm^3\ g^{-1}$)	Nanocrystalline size[c] (nm)
MnO	146	0.29	5.0
Mn_3O_4	144	0.33	5.6
Mn_5O_8	147	0.33	5.2
Mn_2O_3	39	0.22	20

[a] BET surface area was obtained in the relative pressure range of 0.05-0.3.
[b] Pore volume was calculated at the relative pressure of 0.98-0.99.
[c] Nanocrystalline size was calculated by applying the Scherrer equation to the proper reflection of XRPD patterns.

Table S4. The peak positions and multiplet splittings deduced from Mn 2p and 3s XPS analyses.

Sample	3s[a] (eV)	3s[b] (eV)	ΔE_{3s}[c]
MnO	82.9	88.7	5.8
Mn_3O_4	83.4	88.6	5.2
Mn_5O_8	84.1	88.7	4.6

[a, b] Peaks at lower and higher binding energies, respectively
[c] Multiplet splitting values between the peaks for lower and higher BEs were obtained from the fitted XPS spectra.

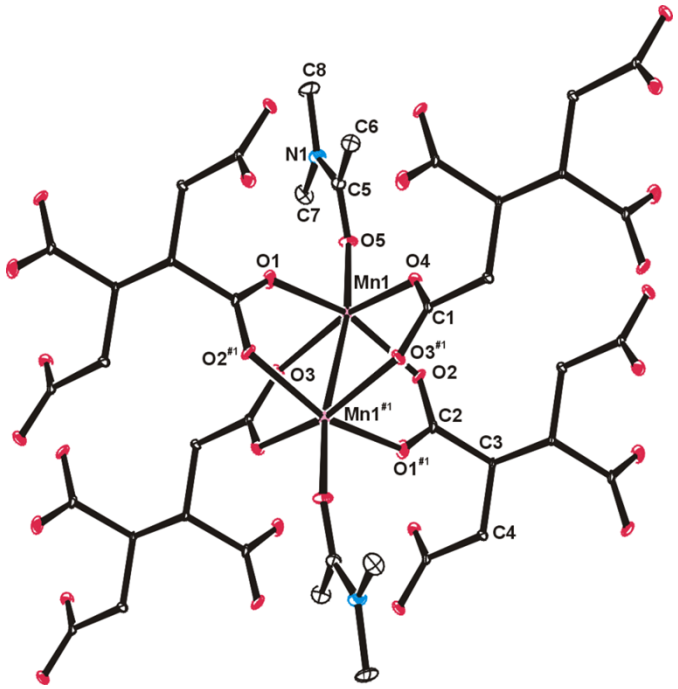

Figure S1. An ORTEP drawing of Mn-MOF with an atomic numbering scheme (thermal ellipsoids at 30% probability). Hydrogen atoms are omitted for clarity. Symmetry operations: $^{\#1}$, -x+2, -y+1, -z+1.

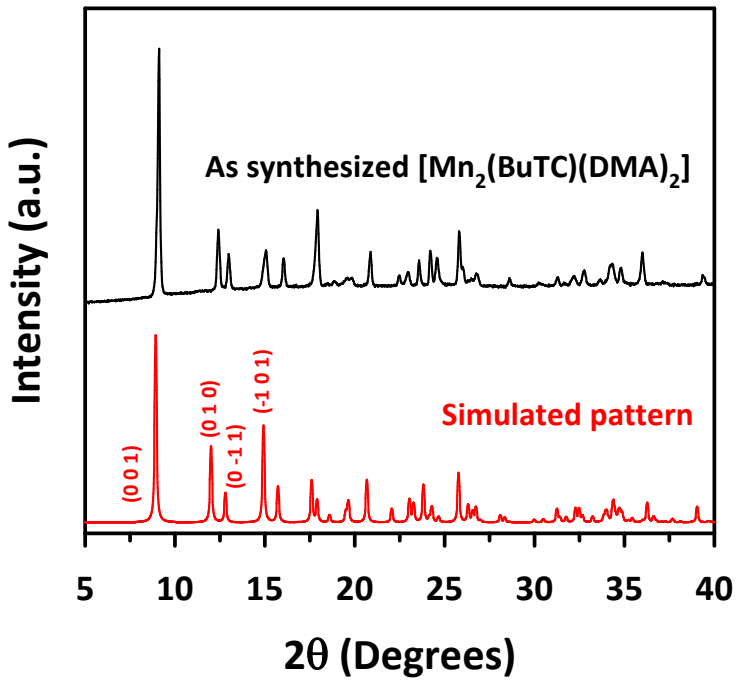

Figure S2. XRPD patterns of Mn-MOF: (a) experimental data and (b) simulated pattern from X-ray single-crystal data.

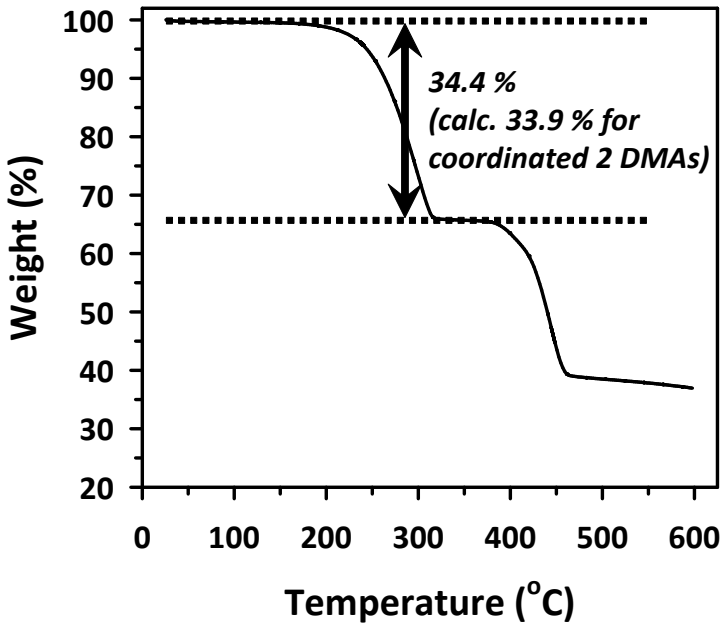

Figure S3. TGA trace of $[Mn_2(BuTC)(DMA)_2]_n$(Mn-MOF). The result indicates that 34.4% weight loss at 200 – 300 °C, corresponding to the loss of 2 DMA molecules (calc. 33.9%), followed by additional weight loss at ~400°C, corresponding to decomposition of Mn-MOF.

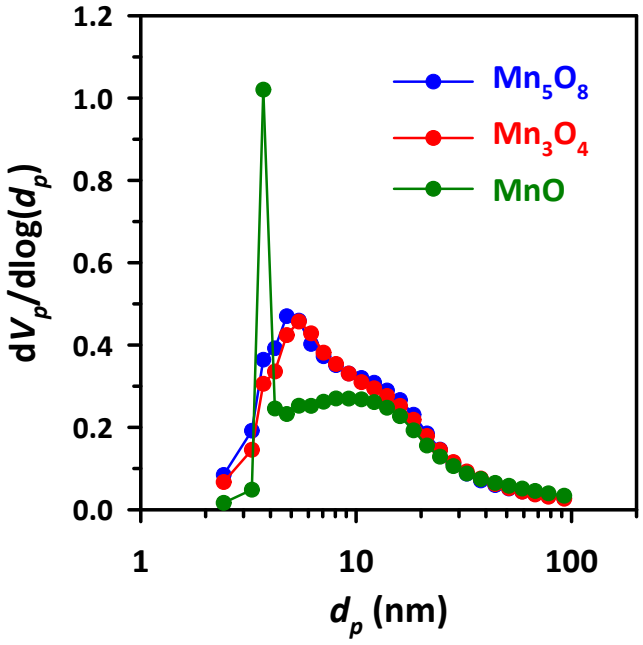

Figure S4. Pore size distribution of the nanoporous manganese oxides obtained by BJH method from desorption branch of N_2 physisorption isotherm

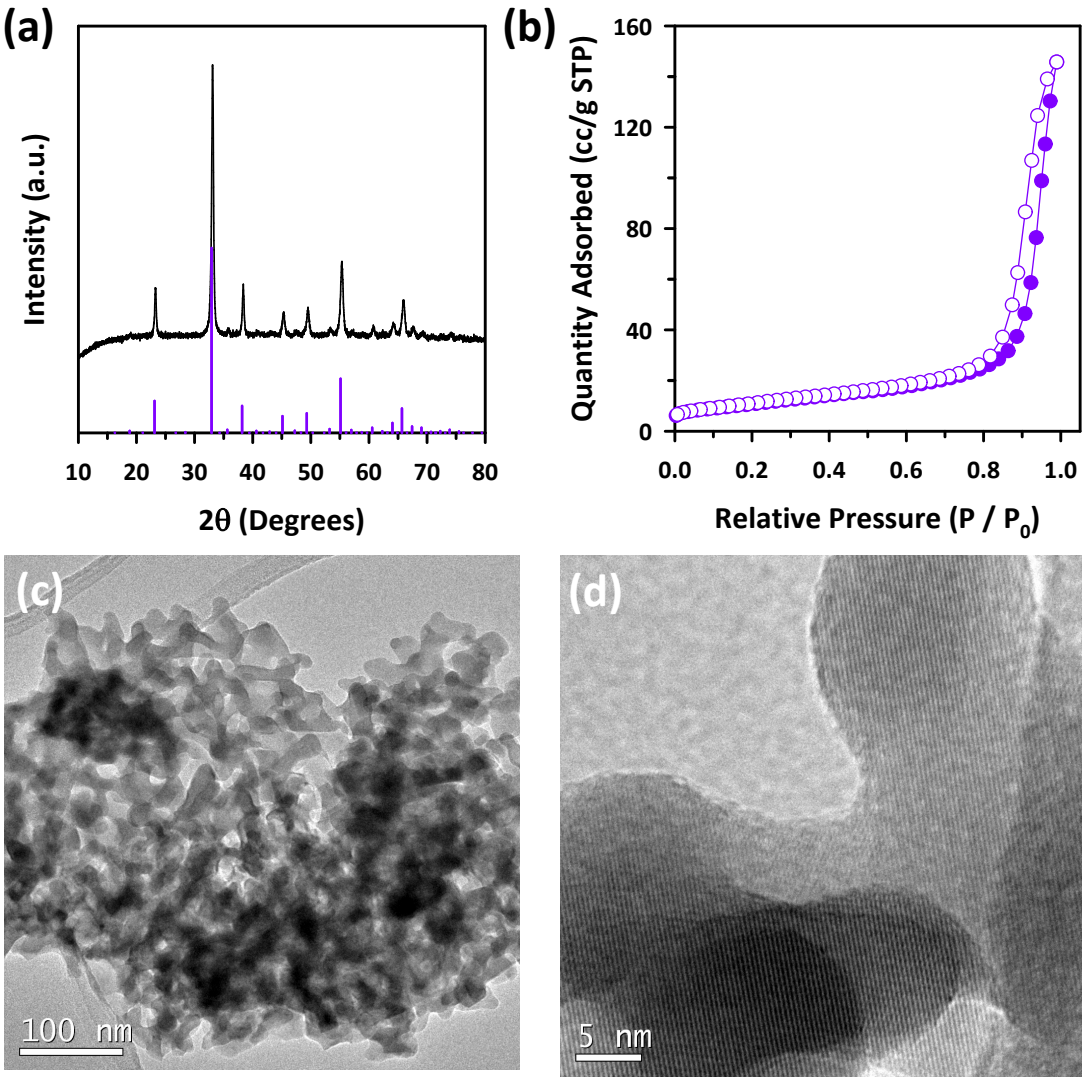

Figure S5. Characterization of an Mn_2O_3 sample: (a) XRPD pattern, (b) nitrogen adsorption−desorption isotherms, and (c,d) TEM images.

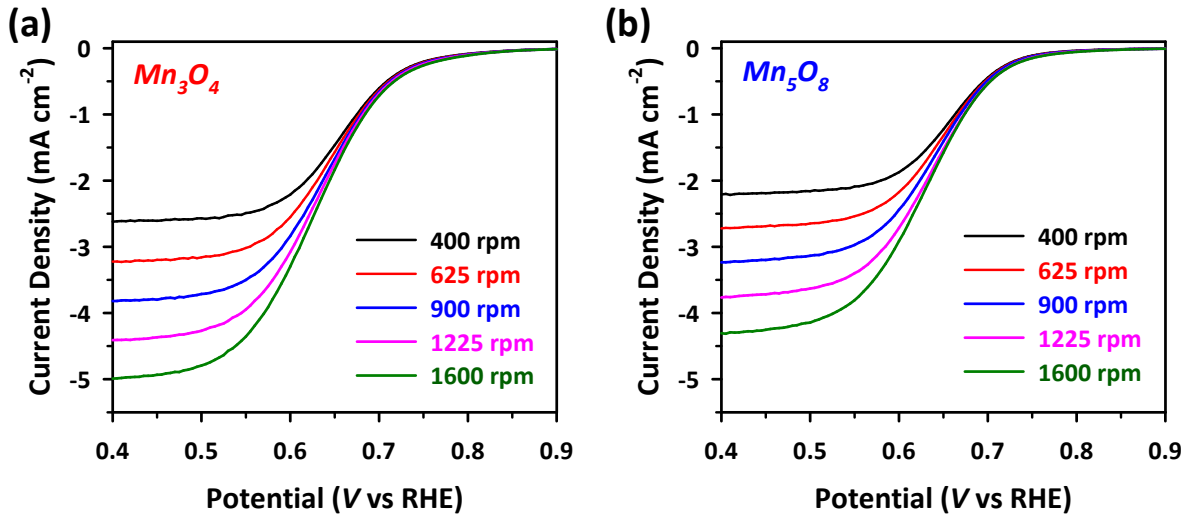

Figure S6. LSV polarization curves for the ORR measured at different rotating rates: (a) nanoporous Mn_3O_4, and (b) nanoporous Mn_5O_8.

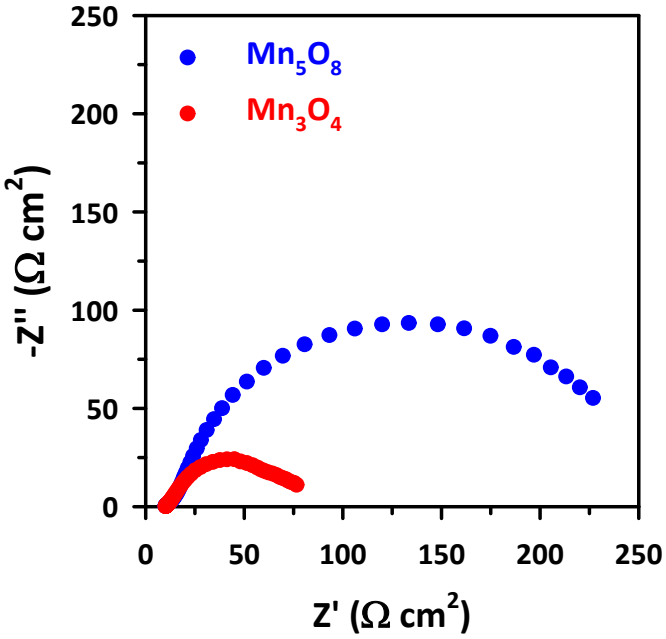

Figure S7. Nyquist plots of the manganese oxide samples obtained by impedance spectra at a fixed potential of 0.7 V (vs. RHE) in O_2-saturated 0.1 M KOH.

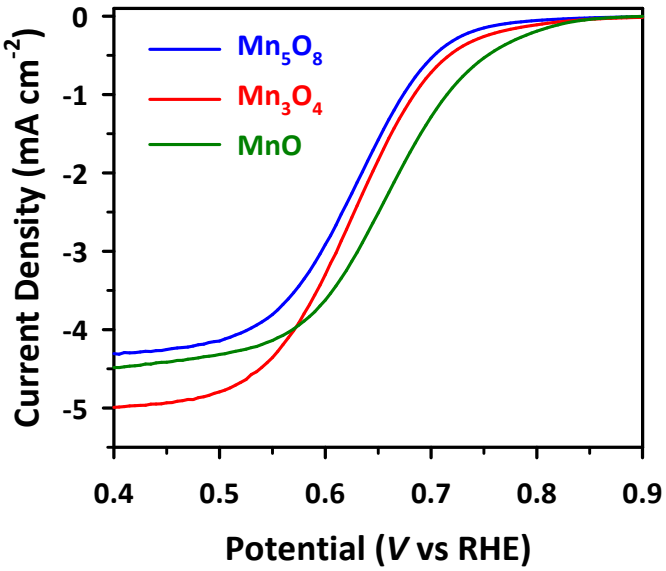

Figure S8. LSV polarization curves for the nanoporous Mn_5O_8, Mn_3O_4, and MnO measured at 1600 rpm in O_2-saturated 0.1 M KOH